Journal of Applied Fluid Mechanics, Vol. 17, No. 11, pp. 2411-2423, 2024.
Available online at www.jafmonline.net, ISSN 1735-3572, EISSN 1735-3645.
https://doi.org/10.47176/jafm.17.11.2596

Experimental Study of Airfoil Aerodynamic Behavior under Oscillating Motion in Ground Effect

M. Hadi Doolabi†, M. Bakhtiarifar and H. Sadati

Aerospace University Complex, Malek Ashtar University of Technology, Tehran, Tehran, 15875-1774, Iran

†*Corresponding Author Email: mhadidoolabi@mut.ac.ir*

ABSTRACT

When a flying vehicle approaches a water or land surface, it induces changes in the fluid flow field pattern known as the "ground effect." This research analyzes the ground effect phenomenon, exploring its impact on aerodynamic coefficients and flow patterns around the NACA0012 airfoil in an incompressible subsonic regime under static and dynamic conditions with pitch movements. Numerical simulations and experimental testing in an incompressible subsonic wind tunnel were deployed. The flow field solution is derived from the Navier-Stokes equations, incorporating the Transition SST turbulence model. Initially, the impact of the ground effect phenomenon was investigated at varying distances from the surface in the static state. Subsequently, the airfoil underwent a sinusoidal pitching oscillation at each distance with a specified frequency and amplitude. This allowed for examining its aerodynamic characteristics over time. The static analysis results reveal alterations in the curve's behavior and pressure distribution on the airfoil surface at close distances to the surface. This is attributed to the ground effect phenomenon, which reduces lift force to a certain height and then increases. Dynamic analysis further demonstrates changes in lift coefficient oscillation amplitude. It also exhibits a minimum and maximum lift point phase difference as the airfoil approaches the surface.

Article History

Received January 18, 2024
Revised May 10, 2024
Accepted May 14, 2024
Available online September 1, 2024

Keywords:

Ground effect
Subsonic
NACA0012
Pitching
Experimental
Numerical solution

1. INTRODUCTION

As a flying vehicle approaches the surface, whether water or ground, flow field patterns change during flight. These changes directly affect the aerodynamics and control of the flying vehicle, necessitating careful consideration to ensure continued movement. This is particularly crucial during the phases of landing and taking off, and flying at low altitudes. When a wing flies in free flow, the upper surface experiences reduced air pressure, while the lower surface encounters comparatively higher pressure, generating lifting force. Researchers discovered that flying near boundaries amplifies air pressure on the lower wing surface. This renders it more aerodynamically efficient than flying freely or farther from boundaries. The combination of these effects leads to a phenomenon known as the "ground effect" (Liang et al., 2013; Sereez et al., 2017; Srivastava, 2019; Baddoo et al., 2020; Zhu et al., 2021).

Ground effect can be classified into two distinct regimes: ram and normal ground effect (Husa, 2000). Ram ground effect is observed where the wing is at an altitude of 0.1 times the airfoil chord or less. In this respect, the wing is positioned so close to the ground that the trailing edge creates a sealed envelope. The airfoil operates within a trapped air cushion, like a hovercraft. As the airfoil's altitude increases, it enters what is typically considered a normal ground effect. This regime extends from just above the "ram wing" height (height greater than 0.1 airfoil chord) to approximately half the wingspan above the ground (Zerihan & Zhang, 2000).

When a wing is positioned near a surface at a distance less than half its span length, two notable changes in its aerodynamic behavior become evident. One is an increase in lift and a decrease in roiling, leading to an increased lift-to-drag ratio. This phenomenon is collectively called the ground effect (Srivastava, 2019). The heightened lift results from the entrapment and compression of air between the wing's bottom surface and the adjacent surface. This is like air creation beneath the wings.

On the other hand, as the aircraft approaches the surface, the wingtip vortices weaken compared to flying in free flow away from the surface. Consequently, the downwash on the wing decreases, increasing the effective angle of attack. The reduction in drag can be attributed to the diminished impact of wingtip vortices and induced

NOMENCLATURE

c	average airfoil chord	U	flow velocity
Cd	coefficient of drag force	∞	unlimited
Cl	coefficient of lift force	V	air velocity
Cm	coefficient of pressure	k	reduced frequency
Cp	coefficient of pressure	α	angle of attack
h	height of the trailing edge of the airfoil to the surface below it	α_a	amplitude of the oscillating attack angle of the dynamic motion of the pitching
l	airfoil length	α_0	mean value of attack angle
P	pressure	ω	angular oscillation velocity
t	time	T	periodicity
Re	reynolds number		

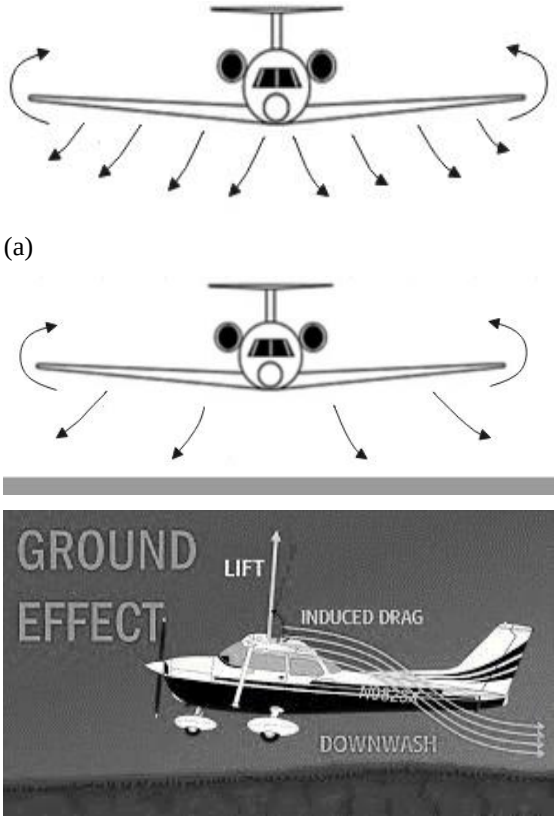

(a)

(b)

Fig. 1 (a) Wingtip vortices far from the ground, (b) wingtip vortices near the ground

drag, ultimately resulting in decreased total drag. Figure 1 (a, b) depicts the flow patterns near and far from the surface, respectively (Holloran & O'Meara, 1999; Liang et al., 2013; Zheng et al., 2019).

A practical example of the ground effect phenomenon is observed in Wing-in-Ground (WIG). WIG crafts are distinctive vehicles that operate at altitudes several meters above the sea surface, taking advantage of favorable aerodynamic interactions between the Wing and the ground (Winarto et al., 2002). The Wing-in-Ground (WIG) craft (Rozhdestvensky, 2006) is designed to capitalize on the ground effect at low altitudes, enhancing flight efficiency, particularly for high-speed sea transportation. It boasts rapid speed and reduced drag compared to traditional ships. It also offers a higher lift-to-drag ratio and energy utilization efficiency than conventional aircraft. However, the WIG craft exhibits distinctive aerodynamic features when operating close to the ground, differing significantly from conventional aircraft. Therefore, numerous scholars have researched these unique aerodynamic characteristics of the WIG craft (Hsiun & Chen, 1996; Lange & Moore, 1980; Ockfen & Matveev, 2009; Jamei et al., 2012; Jung et al., 2012a, b; Qu et al., 2014).

The WIG craft is designed to fly at low altitudes. However, it faces numerous obstacles on land, including buildings, trees, and hills. The vast, flat ocean surface presents an ideal scenario for WIG craft to operate at low altitudes. This makes it suitable for sea transport. The ground effect phenomenon during aircraft landing and take-off, especially in those with high aspect ratio wings, has been extensively studied (Liang et al., 2013; He, 2014).

The historical background of this phenomenon dates back to before 1920 AD. This coincided with the flight of the first airplanes and the initial reports of the ground effect phenomenon by pilots. These reports indicate a general decrease in drag force and an increase in lift force during aircraft landing and take-off. In 1922, Weisler Berger conducted experimental and theoretical studies on the ground effect. Subsequently, various experiments were performed to study this phenomenon, often involving the placement of a flat plate near the wing in wind tunnels. In the 1920s, the actual VE-7 (Fig. 2) was completed at a high altitude, continuing Weissler Burger's work. The results indicate a reduced drag force on the aircraft near the surface.

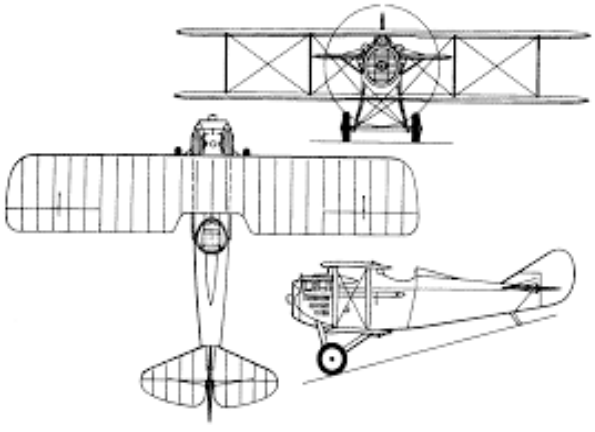

Fig. 2 VE-7: an early biplane

Fig. 3 X-112 airfoil boat

In the 1960s, in the former Soviet Union, WIGs were developed by the Head Office of Hydrofoil Design, headed by Rastsila and Alexiev. Attempts to construct a high-speed sea transport vehicle, led by Alexei, ultimately resulted in WIGs in Russia. Significant progress was made in the United States. Alexander Lippisch, now recognized as the father of delta-wings, conducted tests on his ground effect float called X-112, as shown in Fig. 3. Winarto et al. (2002) studied airfoil geometry in the ground effect phenomenon. They analyzed two types of airfoils, DHMTU 12-35.3-10.2-80.12 and NACA0012, in wind tunnels, highlighting their strengths and weaknesses. This study aimed to optimize airfoils for ground effect.

In another study, Tracy Barber et al. delved into the ground effect phenomenon, employing experimental and numerical methods. Observing airflow patterns within the numerical solution, they identified crucial items and parameters for consideration in experimental tests, including the simulation of ground motion using a conveyor belt to eliminate the effect of the static surface boundary layer on the pressure distribution around airfoil surfaces near the ground. They also emphasized correctly implementing boundary conditions in both experimental and numerical contexts and found the substantial influence of viscous effects on the ground effect (Barber, 2006).

In 2004, Ahmed Rafiuddin conducted experimental investigations on NACA0015, 4415, and 6415 airfoils, creating multiple pressure points. He recorded the corresponding pressures. Utilizing specific equipment, he held the model very close to the surface. A notable shortcoming in his work was the boundary layer created by the stationary surface beneath the model, affecting the flow around the model in the context of the ground effect phenomenon (Ahmed, 2004).

Meanwhile, Zhang et al. at the University of Southampton investigated a wing with a flap near the surface of a wind tunnel. Their findings indicated quasi-two-dimensional flow in approximately half the wing's width, and they further explored the effect of the flap and its angle changes near the surface (Zhang & Zerihan, 2003).

Smuts and Sayers (2011) studied ground effects using the Fluent program. They modeled both level and uneven ground conditions, focusing on the DHMTU 10-40-2-10-2-60-21-5 airfoil. Tahani et al. (2014) conducted a numerical study investigating the effects of geometric changes on the aerodynamic characteristics and static stability of the floating ground effect. They achieved favorable results by numerically examining the wing with a NACA6904 airfoil and comparing the results with similar experimental tests. Baddoo et al. (2020) delved into research on the ground effect phenomenon, obtaining several exact solutions and elucidating the underlying physical mechanisms involved in ground effect. Jing Feng et al. (2022) explored the ground effect phenomenon and its impact on the performance of three straight rectangular models by using a numerical solution (CFD). They applied the results to aircraft control and stability. Shi et al. (2022) investigated the effect of the ground effect phenomenon on supersonic nozzle performance. They conducted a numerical analysis of the aerodynamic characteristics of a supersonic nozzle in the presence of ground effect.

Studies show that the primary research in the ground effect field is related to examining airfoil geometric parameters and flow parameters. This is to investigate the effects of airfoils' aerodynamic behavior in static mode. Notably, the study of airfoils with oscillating movements near the surface has never been considered.

2. METHOD

2.1 Subject Definition

A cambered wing in the ground effect possesses many aerodynamic features of both practical and fundamental interest. Despite recent research regarding the Wing-in-Ground effect, there are still significant gaps in the fundamental aerodynamic understanding of the topic (Zerihan & Zhang, 2000).

In this research, numerical solutions and experimental tests investigated the aerodynamic behavior of a two-dimensional wing section with oscillating pitching motion near the surface. Since flying vehicles and plane surfaces typically have wings with high aspect ratios due to flight continuity, oscillating movements in the wings are inevitable. This is due to the lack of rigidity in the structures. These movements usually involve pitching, plunging (up and down) or combining these motions. The interactions between the phenomena governing these unsteady oscillating movements and those governing the ground effect can significantly influence the aerodynamic behavior of the wings. This results in behaviors different from those observed without ground effects. Studying these behaviors is essential for a more detailed analysis of the performance of this type of aircraft near the surface.

When two-dimensional airfoils are positioned near the surface, various aerodynamic behaviors can be observed based on the airfoil curvature, angle of attack, and distance to the surface. This is especially true for the lift force coefficient. For airfoils with a convex bottom surface at a low angle of attack, the situation is similar to that between their bottom surface and the wall resembling a Venturi nozzle. In this scenario, flow velocity increases and pressure decreases, leading to lower lift coefficients. Another scenario involves compression of the flow below

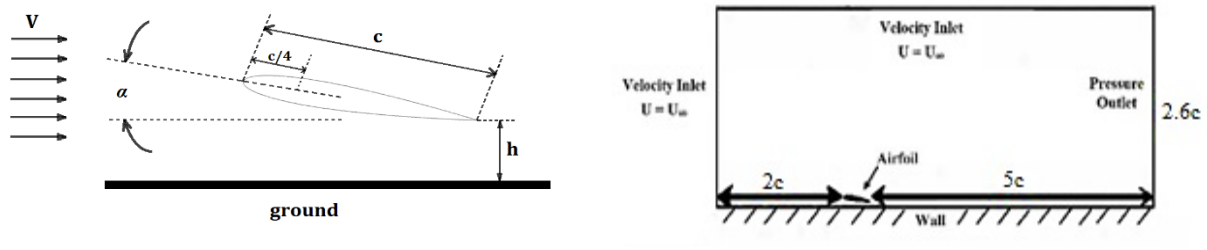

(a) (b)

Fig. 4 (a) Boundary conditions, (b) Dimensions of the solution domain

the airfoil's lower surface. This results in increased pressure and lifting force. This situation is characteristic of airfoils with a flat bottom surface or those positioned at a high angle of attack.

On the other hand, airfoils with oscillating motion exhibit distinct aerodynamic behaviors influenced by airfoil movement. Vortices shed during oscillation and the virtual mass effect. These behaviors are entirely dependent on the dimensionless reduced frequency parameter, as defined by formula (1):

$$k=c\omega/V \quad (1)$$

Where ω presents the angular oscillation velocity (radians per second), V is the flow velocity (meters per second), and c is the average airfoil chord (meters).

In this study, the Reynolds number of 3×10^5 is utilized, with the corresponding reduced frequency (k) value set at 0.026, the mean angle of attack is equal to zero, and the oscillation amplitude is set at 1 degree. The installation location of the model in the experimental test and the torque measurement are positioned at a distance of *c/4* from the airfoil leading edge.

The main subject of the present study is to investigate the aerodynamic behavior of a two-dimensional wing section during pitching oscillation motion in the ground effect. The NACA0012 airfoil is chosen as the reference, with apparent symmetry, medium thickness, and a convex bottom surface. Thus, various distances from the surface are considered to examine the Venturi and ram pressure effects on the airfoil's bottom surface. On the other hand, previous studies have extensively explored the unsteady aerodynamic behavior of the NACA0012 airfoil during pitching oscillation motion. This can serve as a basis for validating the unsteady results obtained in this research, particularly in a no-ground-effect situation.

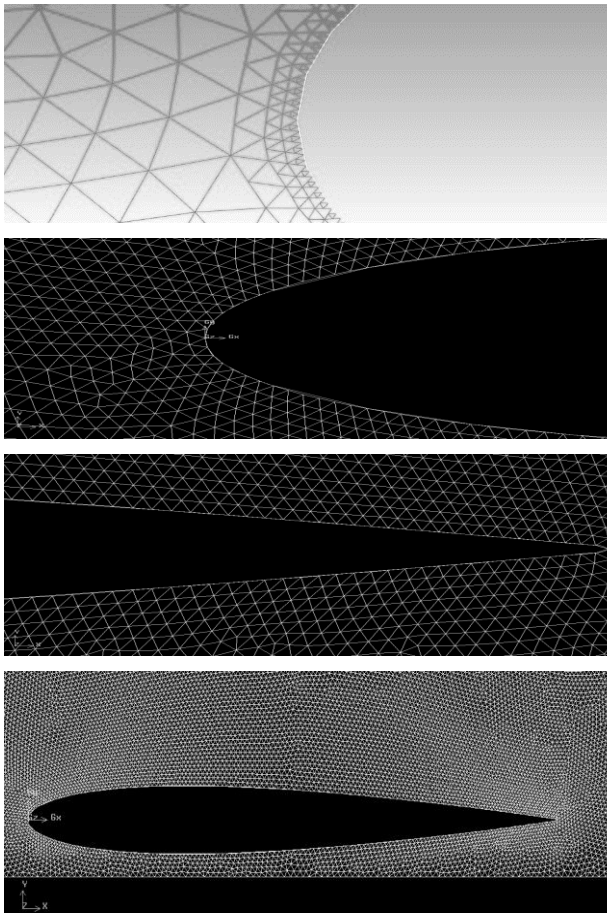

Fig. 5 Unstructured triangular domain mesh for NACA0012 airfoil at zero angle of attack and *h/c*=0.1 (Showing the airfoil with a zoomed view of the leading and trailing edge of the airfoil before solving)

2.2 Numerical Study

In addition to the experimental study, numerical commercial software (FLUENT) has been deployed to analyze the problem. The flow field model, dimensions, and boundary conditions align with 4 (a, b). The distance of the airfoil from the ground (h), measured from the trailing edge to the ground in the static state, is shown. The airfoil chord (c) is assumed to be 0.15 m.

The boundary conditions of the solution domain are such that the input boundary condition is velocity-inlet, the output boundary condition is pressure-outlet, the lower boundary condition is wall for simulating the ground, and the upper boundary condition is velocity-inlet.

The modeled airfoil and its surrounding mesh are shown in Fig. 5. The generated mesh is suitable for measuring the boundary layer on the airfoil and ground surface. Within the field, a triangular disorganized mesh (unstructured) has been utilized. To enhance the modeling of the boundary layer on the airfoil surfaces, three layers of adaptation were created before solving in Fluent software.

The pitching oscillation motion model for the airfoil is described by formula (2):

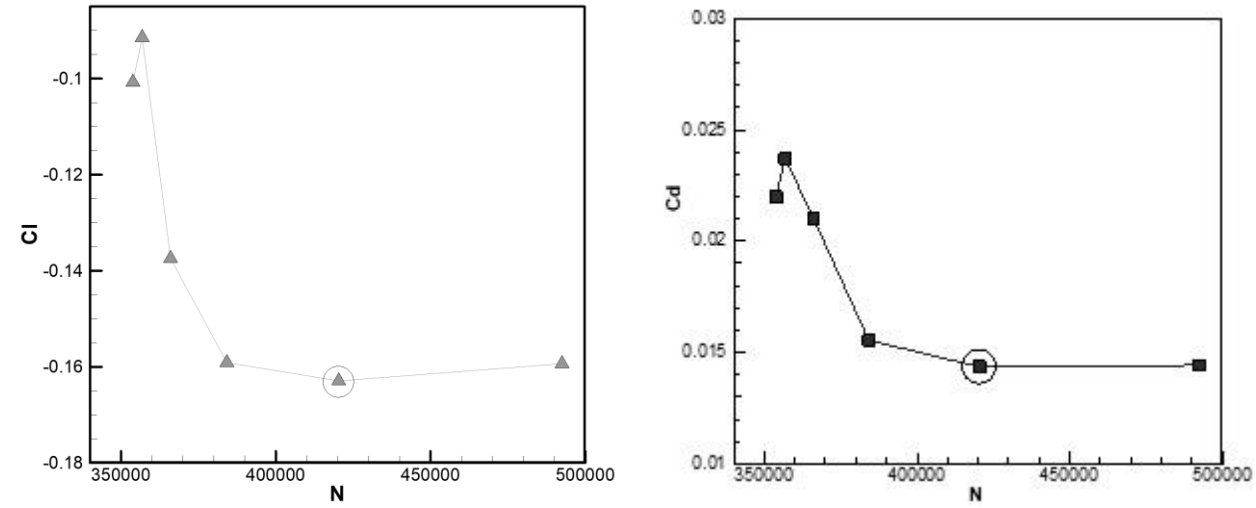

(a) (b)

Fig. 6 Investigation of the dependence of the answer on the number of network elements. (a) *Cl* value according to the number of meshes, (b) *Cd* value according to the number of meshes

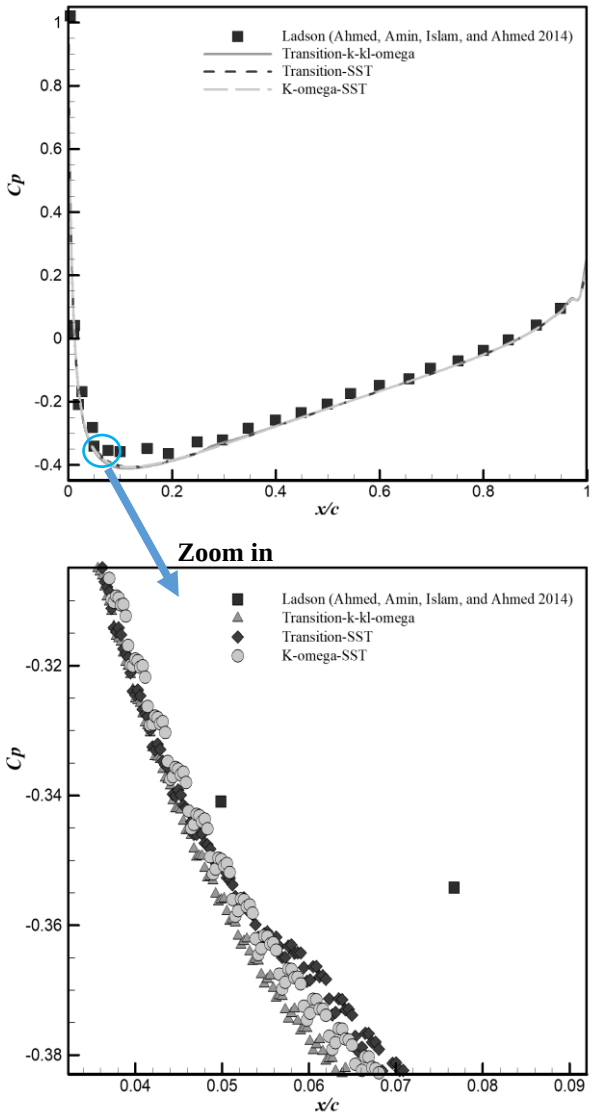

Fig. 7 Investigation of the pressure coefficient dependence on the turbulence model (Reynolds number 6 million and zero angle of attack, no ground effect)

$$\alpha=\alpha_0+\alpha_a \sin(\omega t) \quad (2)$$

Where α_a is the amplitude of the oscillating attack angle during the dynamic pitching motion (degree), and α_0 is the mean value of α (degree) representing the angle of attack before the start of the dynamic motion.

To ensure the quality of the grid, a grid study is performed for the NACA0012 airfoil under flow conditions with $Re=2\times10^6$, $\alpha=0$, and $h/c=0.2$. The variations in lift and drag coefficients with the number of grid elements are depicted in Fig. 6 (a, b). It is observed that there is no significant alteration in lift and drag coefficients for grids exceeding 420,345. This grid is used for numerical studies.

A turbulence model study has also been conducted, and the results are summarized in Fig. 7. As shown in Fig. 7, the pressure coefficient obtained from the Transition SST solution model is in reasonable agreement with Ladson (Ahmed et al., 2014) and is suitable for near-surface conditions with a low Reynolds number. Therefore, this turbulence model will be used in this research. The type of solver is "pressure-based" and the velocity formulation is "absolute". The energy equation is active. The solution model is based on "coupled" and "second order". The solution settings in dynamic modeling are such that the "smoothing" and "remeshing" options are active.

The results in the reference (Ockfen & Matveev, 2008) for the NACA4412 airfoil in ground effect have been used to validate and verify the modeling process and establish the correct solution parameters. This airfoil is cambered with a relatively flat bottom surface. Fig. 8 (a) compares the pressure distribution on the upper and bottom surfaces of this airfoil with the findings presented in the reference (Ockfen & Matveev, 2008). The airfoil is located at a distance of $h/c=0.1$ from the surface and has an angle of attack of 5 degrees. There is substantial agreement between the present results and the reference data. To show the effects of the ground on the pressure distribution around the airfoil, the pressure distribution

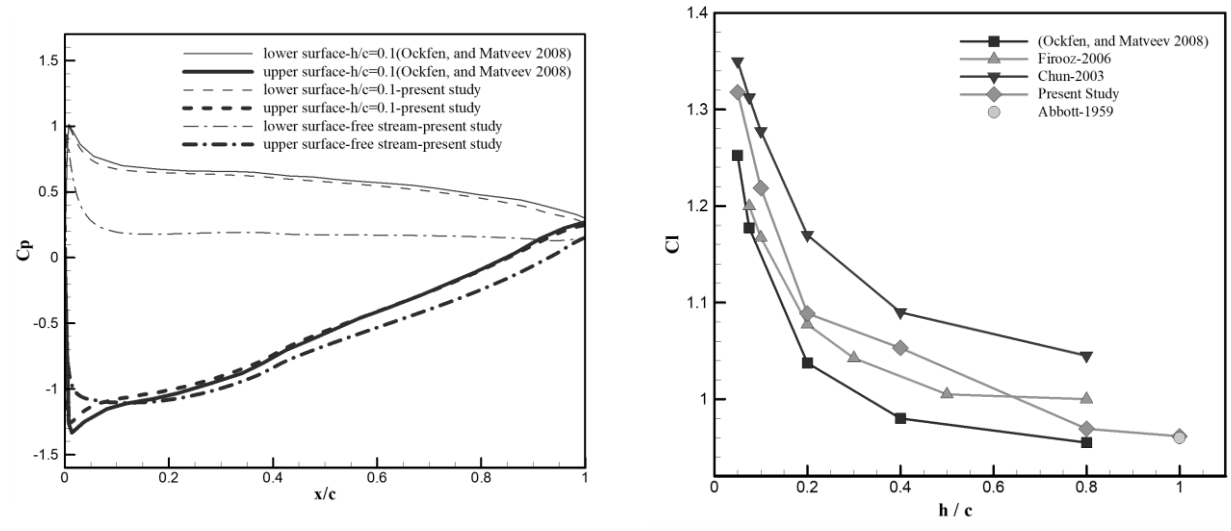

(a) (b)

Fig. 8 (a) Comparison of NACA4412 airfoil numerical solution results at h/c=0.1, α=5° and Re=2×10^6, (b) Comparison of NACA4412 airfoil numerical solution results at α=5° and Re=2×10^6

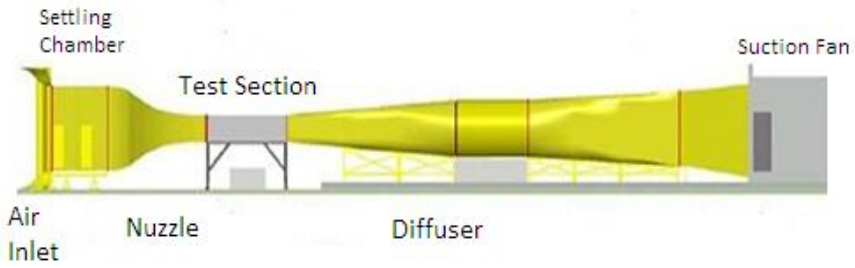

Fig. 9 Wind tunnel scheme

results around the airfoil without the ground effect is also demonstrated in Fig. 8 (a) (free stream) and Fig. 8 (b) (abbott-1959). As can be seen, flow compression occurs on the airfoil's lower surface, increasing pressure. This pressure increase on the lower surface increases the lift coefficient adjacent to the surface. The results of these changes in the lift coefficient in Fig. 8 (b) is compared with different references' results in terms of distance.

3. EXPERIMENTAL STUDY

Researchers still use experimental investigations, as experiments can serve as benchmarks for numerical and theoretical analyses.

A wind tunnel test has been deployed to analyze the flow field around this airfoil in the context of the ground effect phenomenon. All tests are conducted in an open-circuit, suction-type, low-speed wind tunnel. The test section dimensions are 80 cm × 100 cm, with an operating speed range of 5 to 95 m/s and a turbulence intensity of less than 5%.

Fig. 9 illustrates the wind tunnel scheme.

Figure 10 (a) shows a configuration of 11 tubes installed in the test section. Figure 10 (b) illustrates the measurement of velocity changes within the test section using an 11-tube pit-static with an air velocity inside the wind tunnel of 30 m/s. The rake was horizontally mounted in the test section and moved in the X and Z directions. The separation distance between each probe on the rake is 8 cm.

This study utilized a NACA0012 airfoil with a length of 0.6 m and a chord of 0.15 m. Figure 11 (a, b) visually represents the airfoil model used, indicating the position of pressure points prepared on its upper and lower surfaces. Additionally, Fig. 12 shows the coordinates of the pressure points considered on the airfoil surface.

To prepare the ground effect phenomenon simulator in the wind tunnel using the stationary surface method, the ground effect phenomenon simulation plate, as illustrated in Fig. 13 (a), was installed in the wind tunnel test section. Several modifications were made to the plate to minimize the boundary layer effect and ensure suitable and uniform flow. These modifications included angling the plate by 2° against the flow and adding a wedge piece in front of the plate. Fig. 13 (b) depicts the boundary layer rake used in this test, and in Fig. 14, the results of the boundary layer measurements on the plate's surface before and after the changes are presented.

The airfoil's surface pressure at various points is transmitted to the pressure sensors outside the wind tunnel through flexible pressure hoses. This is illustrated in Fig. 13 (c). The pressure sensors used are relative pressure gauges manufactured by Honeywell; an example can be seen in Fig. 13 (d).

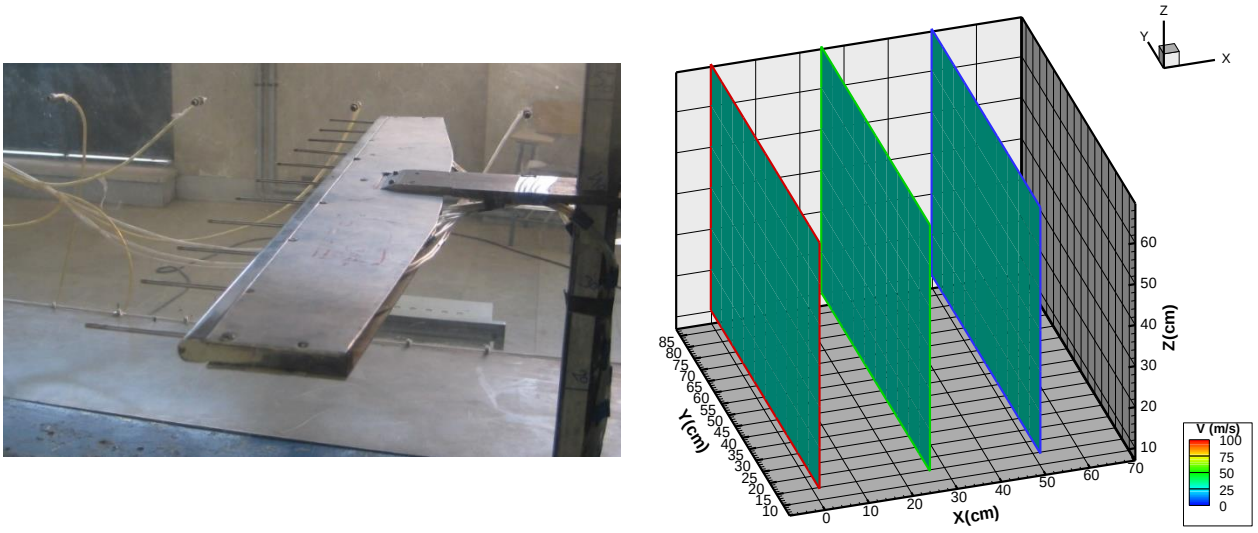

(a) (b)

Fig. 10 (a) Tube pit-static rake, (b) Contour of speed changes inside the test section at 30 m/s start-up speed

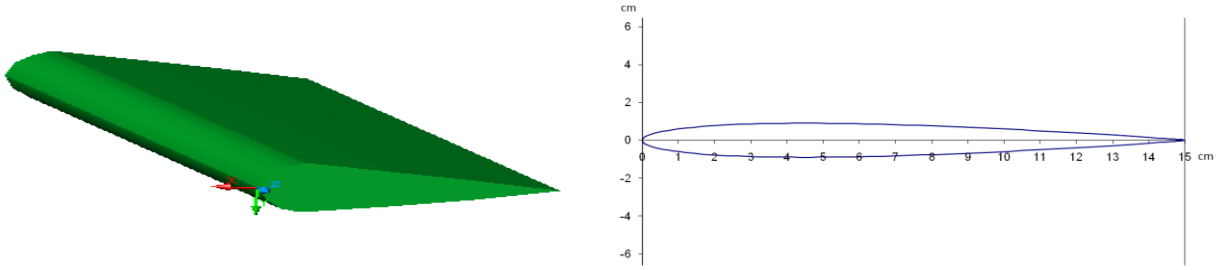

(a) (b)

Fig. 11 (a) Three-dimensional and (b) two-dimensional views of the NACA0012 airfoil model

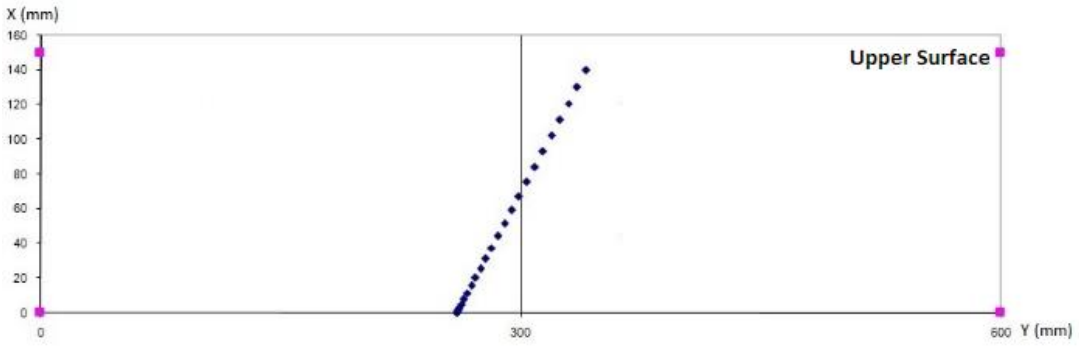

(a)

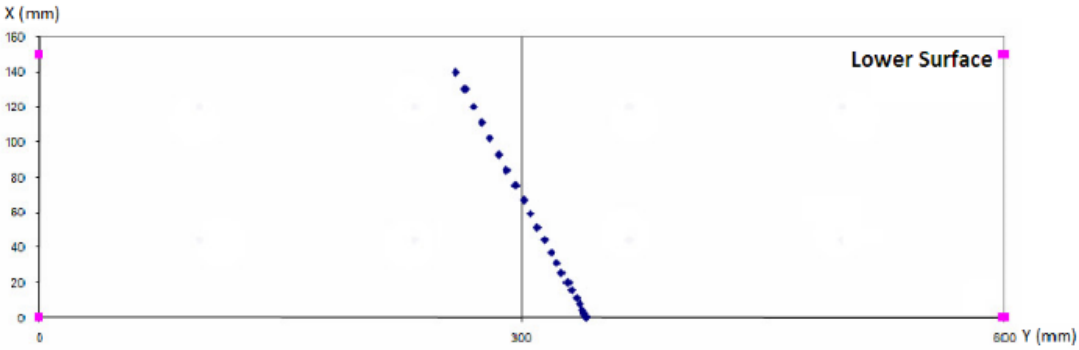

(b)

Fig. 12 Location of pressure points on the surface of the airfoil (*c*=0.15m) (a) upper surface, (b) lower surface

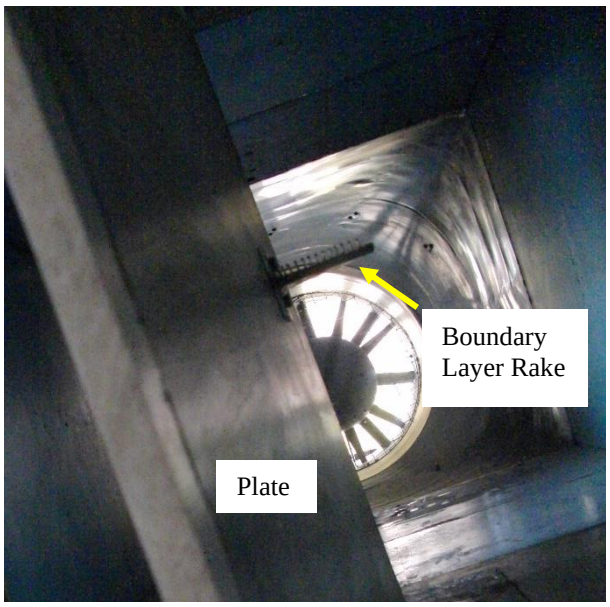

(a)

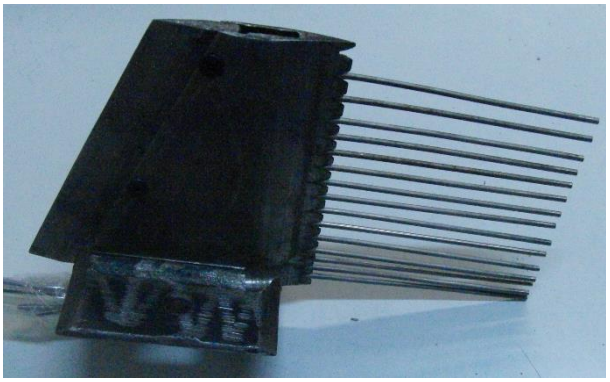

(b)

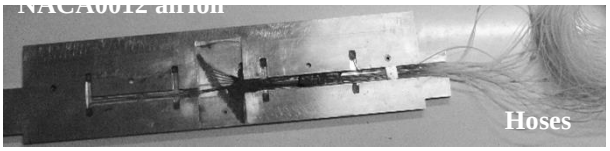

(c)

(d)

Fig. 13 (a) The ground effect phenomenon simulator plate in the test section along with the boundary layer rake, (b) Boundary Layer Rake, (c) Hoses installed on NACA0012 airfoil model to measure the pressure value, and (d) Honeywell 140PC series pressure sensor

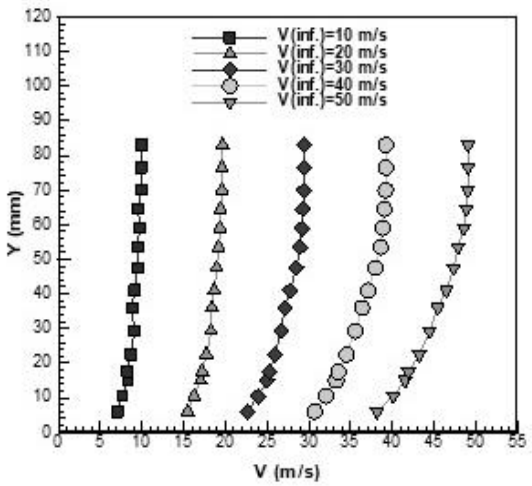

(a)

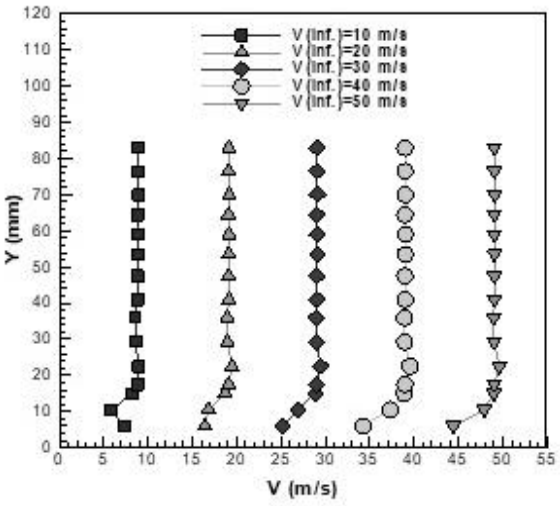

(b)

Fig. 14 Boundary layer changes before (a) and after (b) plate modification at different flow velocities inside the test section

Fig. 15 Installation of the NACA0012 airfoil model near the plate in the wind tunnel test section

In Fig. 15, it is evident that the plate modification has been effective. At various speeds, the boundary layer thickness on the plate has decreased from about 6 cm to 1.5 cm, reaching the desired level. The first distance from

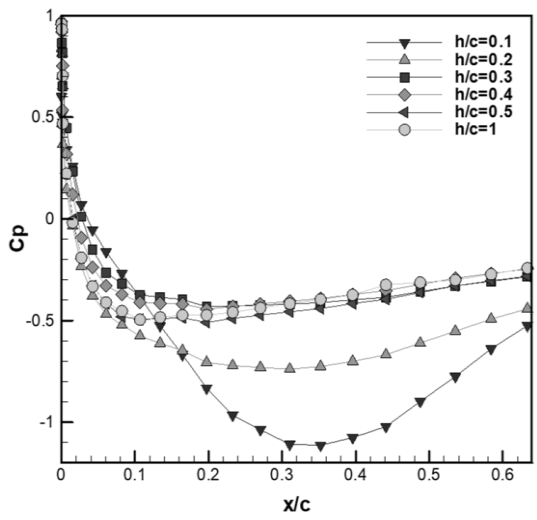

(a)

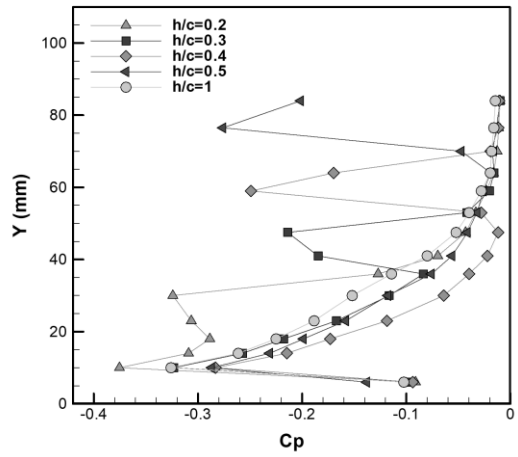

(b)

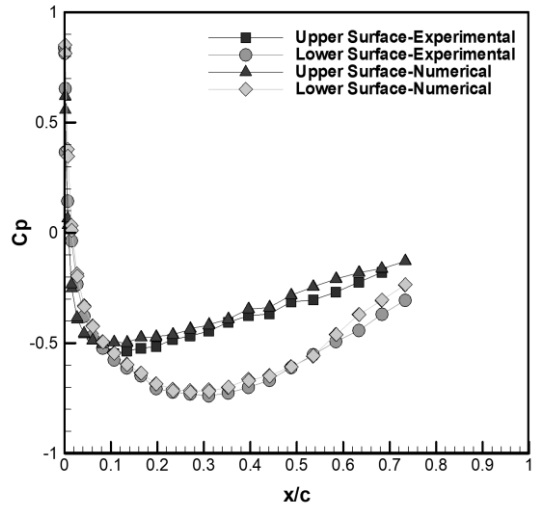

(c)

Fig. 16 (a) Variation of pressure coefficient on the lower surface of NACA0012 airfoil at *v*=30 m/s, *α*=0 and different h/c and static state, (b) Changes in the pressure coefficient measured by the boundary layer rake behind the NACA0012 airfoil at *V*=30 m/s, *α*=0 and different *h/c* and static state, and (c) Comparison the experimental and numerical pressure coefficient results for NACA0012 airfoil at *h/c*=0.2, *α*=0 and *V*=30 m/s

the airfoil's trailing edge to the plate's surface for *h/c*=0.2 is 3 cm, which falls outside the boundary layer impact area. Due to the limitations of the airfoil installation structure in the test section, the application of dynamic motion, and its distance from the boundary layer impact area, preparing h/c values less than 0.2 was impossible. After ensuring that the current formed on the surface was suitable, the model was positioned alongside the plate on the dynamic Alpha mechanism. This is depicted in Fig. 15. This mechanism allows us to swing the airfoil at different attack angles.

The following are the test results of the NACA0012 model in static and pitching oscillating motion. A total of 1000 samples were used for pitching experiments. As shown in Fig. 16 (a), with increasing height from the surface in the static state, the pressure coefficient on the bottom surface of the airfoil reaches its free stream value (*h/c*=1). In this figure, the effects of the airfoil approaching the surface can be observed as decreasing pressure in the middle area of the airfoil. In contrast, increasing pressure is near the leading edge of the airfoil bottom surface. In Fig. 16 (b), changes in the pressure coefficient of the flow behind the airfoil at a distance of 2 cm are observed at different heights. When the airfoil is positioned close to the surface with a low *h/c* ratio, the interaction between the boundary layer and the flow below the airfoil near the surface, which has undergone a static pressure drop, is very strong, leading to a reduction in the pressure on the bottom part of the airfoil due to the interaction of the surface with the airfoil, despite the airfoil's symmetry. With a larger width and height of the plate, this effect and interaction decrease, leaving only the boundary layer effect on the plate.

As can be seen, the wakes formed at the trailing edge of the airfoil at each h/c ratio reduce the pressure behind the trailing edge. The pressure coefficient changes are recorded by the pressure rake and plotted in the corresponding diagram. At each h/c ratio, at the height of the probe rake equal to the distance of the airfoil from the surface, the effect of reducing the wake pressure on the pressure coefficient change is evident, and at higher altitudes, flow recovery occurs, and the measured *Cp* value approaches zero. In Fig. 16 (c), a comparison is presented between the results of an experimental study and numerical investigation on the NACA0012 airfoil at *V*=30 m/s, *α*=0, and *h/c*=0.2. The results reveal an excellent agreement between the experimental and numerical results due to the meticulous setting in the numerical study. Despite the NACA0012 airfoil's inherent symmetry, the pressure coefficient on the upper surface's pressure points is lower than on the lower surface. This is due to the ground effect phenomenon, resulting in a pressure difference that generates lift force.

Figure 17 (a, b) illustrates the results of an experimental test on the pitching oscillating motion of the NACA0012 airfoil at α_0=0, *h/c*=0.2, *k*=0.026, and α_a=1°. There is a satisfactory agreement between numerical and experimental results. The oscillating nature of the pressure coefficient at this point is attributed to the oscillating motion of the airfoil, ultimately causing the aerodynamic coefficients to oscillate. Figure 17 (c) illustrates the changes

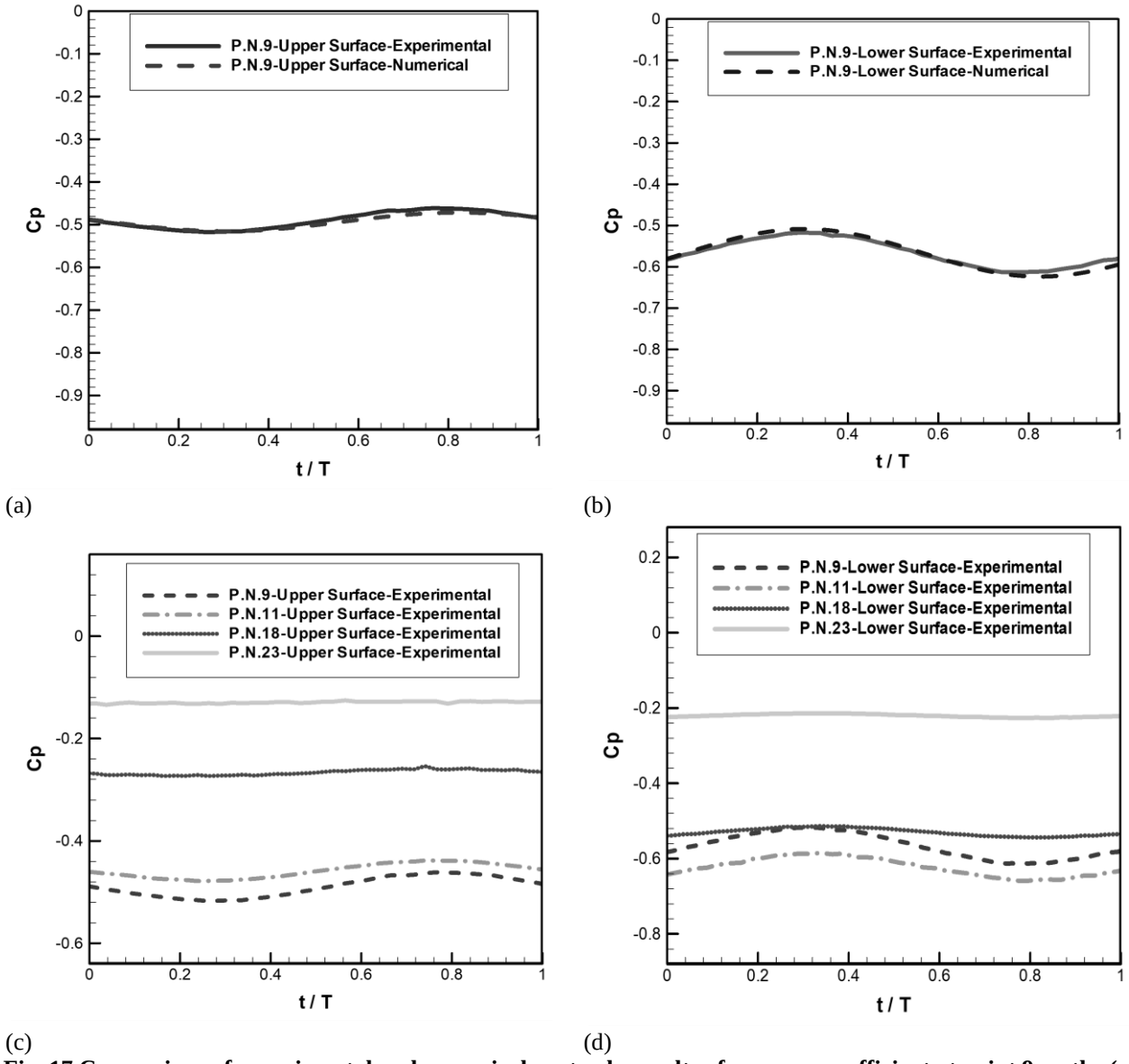

Fig. 17 Comparison of experimental and numerical unsteady results of pressure coefficient at point 9 on the (a) upper and (b) lower surfaces of NACA0012 airfoil at α_0=0, h/c=0.2, k=0.026, and α_a=1º, Results of pressure coefficient on the (c) upper and (d) lower surfaces of NACA0012 airfoil in experimental test at α_0=0, h/c=0.2, k=0.026, α_a=1º and different points, respectively

in the pressure coefficient derived from experimental tests on the oscillating airfoil at α_0=0, h/c=0.2, k=0.026, and α_a=1°, considering the presence of the ground effect phenomenon. When compared to Fig. 17 (d) and the results of the surface below the airfoil, it becomes clear that the pressure changes and their reduction on the lower surface exceed those on the upper surface. This is attributed to the increased impact of the ground effect, and the diagrams exhibit opposing trends and concavities.

The pressure coefficient obtained from the experimental test for the pitching oscillating motion at different points on the lower surface of the NACA0012 airfoil at α_0=0, h/c=0.2, k=0.026, and α_a=1° in the presence of the ground effect is shown in Fig. 17 (d). The airfoil's lower convex shape on the surface reduces pressure. This reduction is more pronounced at the middle points and less in points near the trailing edge. In addition, the pressure changes at the initial points (near the leading edge) are relatively minor than those in the middle and more significant than those at the endpoints (near the trailing edge). This phenomenon is attributed to the formation and recovery of flow on the airfoil surface in the subsonic flow regime.

The aerodynamic coefficients loop from the numerical solution of flow around the NACA0012 airfoil with pitch oscillation motion at α_0=0, k=0.026, and α_a=1° in ground effect with different h/c are shown in Fig. 18 (a, b). At low altitudes, where the ground effect phenomenon is compelling, the Cl coefficient increases and is more significant than at other altitudes. As the plate height increases, the ground effect decreases. This is so that the average Cl coefficient at h/c=1 reaches approximately the amount of free flow, a zero condition for the NACA0012 symmetric airfoil. However, a small positive lifting force is generated due to the pitching oscillating motion. This is

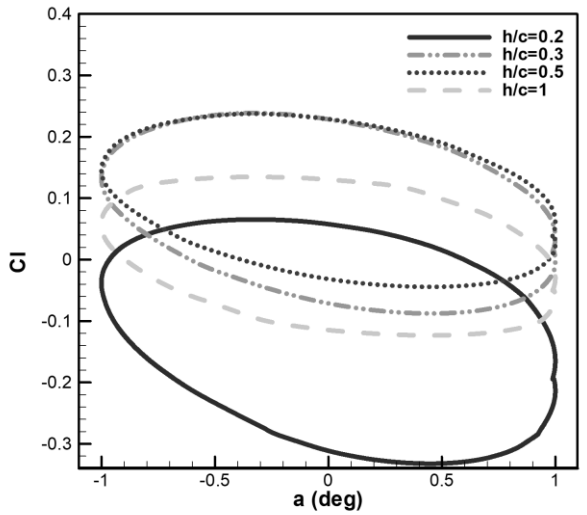

(a)

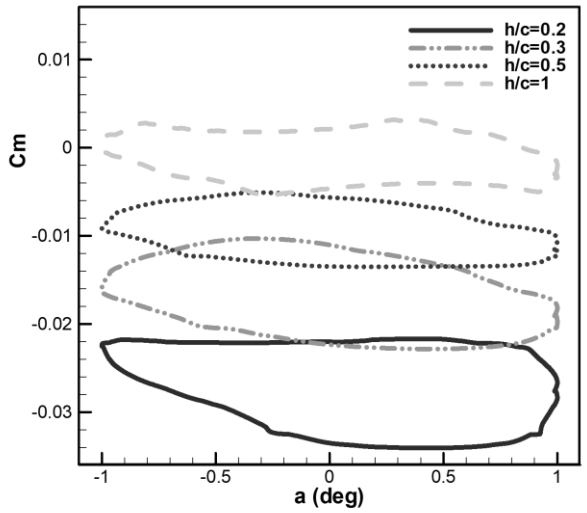

(b)

Fig. 18 Loop of aerodynamic coefficients of NACA0012 oscillating airfoil in different states α_0=0, k=0.026, α_a=1°, and h/c (experimental results). (a) *Cl* values, (b) *Cm* values

due to the flow pattern changes around the airfoil, and the surface pressure is below and above it.

Consequently, the lift force coefficient at h/c=1 may not necessarily be zero. At h/c=0.2, the lift force coefficient is zero at an angle of attack of -0.95° (in the third quarter of the oscillating motion) and 0.6° (in the second quarter of the oscillating motion) due to the airfoil's pitching oscillating motion, its curved and convex shape, and the interaction of the Venturi effect and ground effect. This pressure distribution leads to temporary zero lift. At different altitudes, these angles decrease due to the reduction of the Venturi effect and ground effect, approaching free flow conditions. The lift coefficient increased at h/c=0.5 compared to h/c=0.3 despite the minor amplitude changes attributed to the reduced Venturi effect at that height. At h/c=0.2, the ground effect is prominent as a pitching oscillating motion and a positive angle of attack (0.45°) create a Venturi, resulting in an increased lift value, peaking at -0.35. With a further increase in the angle of attack, the low-pressure area under the airfoil shifts towards the trailing edge, causing a relative decrease in the lifting force. At an angle of attack of 1°, the effectiveness of the low-pressure zone and the Venturi diminishes beyond the airfoil maximum thickness point. During sinusoidal motion and a reduction in the angle of attack, a low-pressure area forms under the airfoil, moving towards the leading edge. The lift coefficient experiences an upward trend until -0.3, followed by a downward trend. Due to proximity to the plate, the ground effect dominates, leading to a relative increase in lift. In sinusoidal motion with an increase in the angle of attack from -1° to zero, the downward trend in the lift coefficient persists, attributed to the ground effect phenomenon.

The airfoil torque is located at point *c/4*. Under pitching oscillating motion at h/c=0.2, as the airfoil approaches the surface, a substantial force is exerted due to the current trapped between the convex lower surface of the airfoil and its bottom plate, leading to an increase in the pitching moment coefficient (*Cm*). At increasing altitude, the force diminishes, reaching an average of approximately zero at h/c=1, indicative of free flow conditions. However, at h/c=1, the oscillating motion causes some negative pitching moment. At h/c=0.2, the maximum pitching moment occurs during motion, attributed to the angle of attack increasing from zero to one. This is influenced by the rotation's location, the proximity of the leading edge to the plate, and current trapping. This results in a lifting force applied to the airfoil's end, creating a negative pitching moment. During the oscillating motion from an angle of attack 0.8° to its upper limit and back 0.8°, the lever effect on the airfoil's forces reduced. This led to a reduction in pitching moments. Despite the oscillations, the pitching moment coefficient remains constant when the angle of attack decreases -1°. This indicates that the applied forces and their points of application remain unchanged. Continuing the oscillations and increasing the angle of attack, the pitching moment coefficient exhibits a decreasing trend relative to the lift coefficient increase. This is attributed to the ground effect efficacy.

4. CONCLUSION

In this research, the aerodynamic behavior of the NACA0012 symmetrical airfoil adjacent to the surface has been studied statically and dynamically with experimental methods and numerical solutions. The correctness of the modeling and the numerical solution method in this work were examined in Figs 6, 7 and 8. In order to establish the flow with the minimum amount of the boundary layer on the surface, the Plate must be flat and have a wedge on the front edge and be placed at an angle of 2 degrees to the vertical axis of the wind tunnel.

As shown in Figs 16(c), 17(a) and 17(b), the results of the experimental method and the numerical solution have a good similarity. The results indicate that height reduction can have varying effects on the lift coefficient for airfoils with lower surface convexity. As the height

from the surface decreases, as shown in Fig. 16(a), the value of *Cp* clearly changes and grows, causing a pressure difference between the lower surface and the upper surface of the airfoil, and naturally, the lift value also increases. This change in pressure caused by the phenomenon of the ground effect in the points on the upper surface and the lower surface of the airfoil is also clear in Figs 17(c) and 17(d).

During the pitching oscillating motion of the NACA0012 airfoil, the pressure coefficient, lift force, and pitching moment exhibit proportionally with the amplitude of motion and reduced frequency of oscillation. When the airfoil pitches near the surface, aerodynamic behavior changes compared to without ground effect. These changes appear as variations in the oscillation amplitude relative to the ground effect condition. As the height from the surface increases, the effect of the surface effect phenomenon decreases and almost from h/c= 0.5, the aerodynamic coefficients do not change and are equal to the free flow conditions (Figures 8(b), 16(a), 17(c) and 17(d)).

This research contributes insights to investigate the aerodynamic behavior of ornithopters and model birds' movement near the surface.

CONFLICT OF INTEREST

This original, unpublished version is not currently considered for publication in other journals. It should also be noted that all authors have approved the manuscript's final version and are aware of this submission. It is also declared that there is no conflict of interest between the authors.

AUTHORS' CONTRIBUTION

Contributions from all authors are equal.

REFERENCES

Ahmed, M. R. (2004). *Flow over thick airfoil in ground effect an investigation on the influence of camber*. Proceedings of the 24th Congress of International Council of the Aeronautical Sciences. https://repository.usp.ac.fj/4420/

Ahmed, T., Amin, M. T., Islam, S. R., & Ahmed, S. (2014). Computational study of flow around a NACA 0012 wing flapped at different flap angles with varying Mach numbers. *Global Journal of Research in Engineering*. https://www.researchgate.net/profile/Shabbir-Ahmed-10/publication/273923634_Computational_Study_of_Flow_Around_a_NACA_0012_Wing_Flapped_at_Different_Flap_Angles_with_Varying_Mach_Numbers/links/551053380cf2ba84483d4c02/Computational-Study-of-Flow-Around-a-NACA-0012-Wing-Flapped-at-Different-Flap-Angles-with-Varying-Mach-Numbers.pdf

Baddoo, P. J., Kurt, M., Ayton, L. J., & Moored, K. W. (2020). Exact solutions for ground effect. *Journal of Fluid Mechanics, 891*, R2. https://www.cambridge.org/core/journals/journal-of-fluid-mechanics/article/exact-solutions-for-ground-effect/A1B93FEDA0A7A8E37711D37BFDBA972A

Barber, T. (2006). Aerodynamic ground effect: A case study of the integration of CFD and experiments. *International Journal of Vehicle Design, 40*(4), 299–316. https://www.inderscienceonline.com/doi/abs/10.1504/IJVD.2006.009068

He, Y. (2014). *Shape optimization of airfoils without and with ground effect using a multi-objective genetic algorithm.* a thesis presented to the School of Engineering and Applied Science of Washington University in partial fulfillment of the requirements for the degree of Master of Science, Saint Louis, Missouri. https://openscholarship.wustl.edu/eng_etds/5/

Holloran, M., & O'Meara, S. (1999). *Wing in ground effect craft review*. Defence Science And Technology Organisation Canberra (Australia). https://apps.dtic.mil/sti/citations/ADA361836.

Hsiun, C. M., & Chen, C. O. K. (1996). Aerodynamic characteristics of a two-dimensional airfoil with ground effect. *Journal of Aircraft, 33*(2), 386-392. https://arc.aiaa.org/doi/abs/10.2514/3.46949

Husa, B. (2000). *WIG configuration development from component matrix*. Orion technology, Aerospace design and engineering, Internal report. https://www.scribd.com/document/580154859/wig-configuration-ekranoplan

Jamei, S., Maimun, A., Mansor, S., Azwadi, N., & Priyanto, A. (2012). Numerical investigation on aerodynamic characteristics of a compound wing-in-ground effect. *Journal of Aircraft, 49*(5), 1297-1305. https://arc.aiaa.org/doi/abs/10.2514/1.C031627?journalCode=ja

Jingfeng, X., Lei, S., Huang, J., & Jingcheng, F. (2022). Parameter study on lateral moments of banked wings in ground effect. *Chinese Journal of Aeronautics, 35*(3) 53-61. https://www.sciencedirect.com/science/article/pii/S1000936121001151

Jung, J. H., Kim, M. J., Yoon, H. S., Hung, P. A., Chun, H. H., & Park, D. W. (2012a). Endplate effect on aerodynamic characteristics of three-dimensional wings in close free surface proximity. *International Journal of Naval Architecture and Ocean Engineering, 4*(4), 77-487. https://www.sciencedirect.com/science/article/pii/S2092678216303648

Jung, J. H., Yoon, H. S., Chun, H. H., Hung, P. A., & Elsamni, O. A. (2012b). Mean flow characteristics of two-dimensional wings in ground effect. *International Journal of Naval Architecture and Ocean Engineering, 4*(2), 151-161. https://www.sciencedirect.com/science/article/pii/S2092678216301972

Lange, R., & Moore, J. (1980). Large wing-in-ground

effect transport aircraft. *Journal of Aircraft, 17*(4), 260-266. https://arc.aiaa.org/doi/abs/10.2514/3.57898?journalCode=ja

Liang, H., Zhou, L., Zong, Z., & Sun, L. (2013). An analytical investigation of two-dimensional and three-dimensional biplanes operating in the vicinity of a free surface. *Journal of Marine Science and Technology, 18*(1), 12-31. https://link.springer.com/article/10.1007/s00773-012-0187-9

Ockfen, A. E., & Matveev, K. I. (2008). *Numerical study of wing aerodynamics in ground proximity.* ASME International Mechanical Engineering Congress and Exposition. https://asmedigitalcollection.asme.org/IMECE/proceedings-abstract/IMECE2008/97/332019

Ockfen, E., & Matveev, K. I. (2009). Aerodynamic characteristics of NACA 4412 airfoil section with flap in extreme ground effect. *International Journal of Naval Architecture and Ocean Engineering, 1*(1), 1-12. https://www.sciencedirect.com/science/article/pii/S2092678216303776

Qu, Q., Jia, X., Wang, W., Liu, P., & Agarwal, R. K. (2014). Numerical simulation of the flow field of an airfoil in dynamic ground effect. *Journal of Aircraft, 51*(5), 1659–1662. https://arc.aiaa.org/doi/abs/10.2514/1.C032452

Rozhdestvensky, K. V. (2006). Wing-in-ground effect vehicles. *Progress in Aerospace Sciences, 42*(3), 211-283. https://www.sciencedirect.com/science/article/abs/pii/S0376042106000637

Sereez, M., Abramov, N., & Goman, M. (2017). *Computational ground effect aerodynamics and airplane stability analysis during take-off and landing.* 7th European Conference For Aeronautics And Aerospace Sciences (Eucass). https://dora.dmu.ac.uk/server/api/core/bitstreams/8bb7e7bd-6789-4e93-a6b2-dbbffde0f838/content

Shi, Y., Chen, L., Chen, P., Yang, Q., Shi, Y., & Yang, H. (2022). *Numerical study on aerodynamic characteristics of supersonic nozzle in presence of ground effect.* Journal of Physics: Conference Series, Publisher: IOP Publishing Pages, 012013. https://iopscience.iop.org/article/10.1088/1742-6596/2252/1/012013/meta

Smuts, E., & Sayers, A. (2011). CFD study of a wing in close proximity to a flat and wavy ground plane. *R & D Journal of the South African Institution of Mechanical Engineering, 27*, 1-9. https://cdn.ymaws.com/www.saimeche.org.za/resource/collection/3FB27C6C-E247-4611-A317-BB0086265083/2011_1_Smuts_and_Sayers_-_FINAL_-_2011,27,1-9.pdf

Srivastava (2019). Determination of aerodynamic forces and control requirements during ground effect. *International Journal of Aviation Aeronautics and Aerospace, 6*(4), 15. https://commons.erau.edu/ijaaa/vol6/iss4/15/

Tahani, M., Bargestan, A., & Sabour, M.H. (2014). Numerical investigation of influence geometry variation on the aerodynamic characteristics and static stability of wing in ground effect. *Journal of Solid and Fluid Mechanics, 4*(2) 75–87. (in Persian). https://jsfm.shahroodut.ac.ir/article_315_en.html

Winarto, H., Amin, I., Sultan, N., Kidane, B., Demircan, O. M., Altinok, A. S., & et al. (2002). *An investigation into wing in ground effect airfoil geometry.* School Of Engineering Sciences, University Of Southampton, SO17 1BJ, UK. https://eprints.soton.ac.uk/51083/

Zerihan, J., & Zhang, X. (2000). Aerodynamics of a single element wing in ground effect. *Journal of Aircraft, 37*(6), 1058-1064. https://arc.aiaa.org/doi/abs/10.2514/2.2711

Zhang, X., & Zeriha, J. (2003). Aerodynamics of a double-element wing in ground effect. *AIAA Journal, 41*(6), 1007-1016. https://arc.aiaa.org/doi/abs/10.2514/2.2057

Zheng, Y., Qu, Q., Liu, P., Qin, Y., & Agarwal, R. K. (2019). Aerodynamics of a two-dimensional flapping wing hovering in the proximity of the ground. *Proceedings of the Institution of Mechanical Engineers, Part G: Journal of Aerospace Engineering, 233*(12), 4316-4332. https://journals.sagepub.com/doi/abs/10.1177/0954410018819335

Zhu, Z. H., Cao, M. S., Xin, Z. Q., & Li, T. (2021). Analysis of fluid and solid interaction of the flexible bionic wing in ground effect. *Proceedings of the Institution of Mechanical Engineers, Part C: Journal of Mechanical Engineering Science, 235*(2), 280-295. https://journals.sagepub.com/doi/abs/10.1177/0954406220935150